INTERNATIONAL JOURNAL FOR NUMERICAL METHODS IN FLUIDS
Int. J. Numer. Meth. Fluids 2008; **57**:1649–1668
Published online 5 December 2007 in Wiley InterScience (www.interscience.wiley.com). DOI: 10.1002/fld.1696

Explicit solution to the exact Riemann problem and application in nonlinear shallow-water equations

Yongyan Wu and Kwok Fai Cheung*,†

Department of Ocean and Resources Engineering, University of Hawaii at Manoa, Honolulu, HI 96822, U.S.A.

SUMMARY

The Riemann solver is the fundamental building block in the Godunov-type formulation of many nonlinear fluid-flow problems involving discontinuities. While existing solvers are obtained either iteratively or through approximations of the Riemann problem, this paper reports an explicit analytical solution to the exact Riemann problem. The present approach uses the homotopy analysis method to solve the nonlinear algebraic equations resulting from the Riemann problem. A deformation equation defines a continuous variation from an initial approximation to the exact solution through an embedding parameter. A Taylor series expansion of the exact solution about the embedding parameter provides a series solution in recursive form with the initial approximation as the zeroth-order term. For the nonlinear shallow-water equations, a sensitivity analysis shows fast convergence of the series solution and the first three terms provide highly accurate results. The proposed Riemann solver is implemented in an existing finite-volume model with a Godunov-type scheme. The model correctly describes the formation of shocks and rarefaction fans for both one and two-dimensional dam-break problems, thereby verifying the proposed Riemann solver for general implementation. Copyright © 2007 John Wiley & Sons, Ltd.

Received 20 June 2007; Accepted 20 October 2007

KEY WORDS: dam-break problem; homotopy analysis method; long-wave equations; shallow-water equations; Riemann problem; Riemann solver

1. INTRODUCTION

The nonlinear shallow-water equations are used extensively to model propagation and runup of long waves, such as tides, storm surge, and tsunamis, as well as open channel and overland flows due to rainstorms or dam collapse. Analytical solutions to these equations are limited to a few special cases and for most practical applications numerical methods are used. The nonlinear

*Correspondence to: Kwok Fai Cheung, Department of Ocean and Resources Engineering, University of Hawaii at Manoa, Honolulu, HI 96822, U.S.A.
†E-mail: cheung@hawaii.edu

Contract/grant sponsor: Office of Naval Research; contract/grant number: N00014-02-1-0903

shallow-water equations are hyperbolic and admit both continuous and discontinuous solutions. Among the numerical schemes, the finite-volume method has the advantage of being able to conserve the basic quantities such as mass and momentum. The Godunov-type schemes based on the solution of a local Riemann problem are robust and accurate in capturing discontinuities such as shocks and contact surfaces. The Riemann solver, which is the basis of these numerical schemes, has gained enormous attention in the research community.

Since there is no close-form solution except for a few trivial initial configurations, a solver is usually sought through approximations of the Riemann problem. In 1981, Roe [1] proposed an approximate solver for the Euler equation through the solution of a linearized Riemann problem. The solver requires an *entropy fix* to capture a sonic or critical rarefaction [2]. The method has been refined and applied to many physical problems in science and engineering. Glaister [3] is one of the first to apply a Roe-type Riemann solver to the nonlinear shallow-water equations and Dodd [4] extended the approach for wave runup, overtopping, and regeneration problems. Hubbard and Dodd [5] implemented the method in two dimensions using an adaptive mesh refinement algorithm, while Bradford and Sanders [6] provided a similar model, but used a characteristic method to track the moving waterline. LeVeque [7] adopted a Roe-type linearization in a quasi-steady wave-propagation algorithm, which is capable of balancing the source terms and flux gradients in high-resolution Godunov methods. Rossmanith *et al*. [8] presented a generalization of the wave-propagation method for hyperbolic systems on a general curved manifold that is high-resolution shock capturing.

An alternate approximate Riemann solver is based on the Osher–Solomon scheme for a general system of hyperbolic conservation laws [9]. The scheme splits the numerical flux into forward and backward vector-valued functions and satisfies the entropy condition for sonic flows. It has been applied by Zhao *et al*. [10] for the nonlinear shallow-water equations in modeling hydraulic shock waves and unsteady flow in river basins. Harten *et al*. [11] suggested another approach for the solution of the Riemann problem through an approximation to the numerical flux by three constant states separated by two waves with constant speeds. Einfeldt [12] proposed algorithms for the computation of the wave speeds. The approach was later referred to as the HLL or HLLE Riemann solver. Toro *et al*. [13] modified the HLL scheme by approximating the flux with four constant states. Using an HLL Riemann solver, Hu *et al*. [14] proposed a one-dimensional shallow-water model for wave propagation, runup, and overtopping, and Zhou *et al*. [15] described a well-balanced model with the surface gradient method.

Even though approximate Riemann solvers can give good results, some researchers opt for the so-called exact solver through some numerical iterative schemes. Brocchini *et al*. [16] applied the finite-volume method to two dimensions using the weighted average flux method with the moving waterline treated as a cavitation problem. Wei *et al*. [17] and Pan *et al*. [18] presented well-balanced finite-volume models with the exact Riemann solver. It should be emphasized that the solver is accurate to a predefined tolerance and is called exact only for differentiation from the approximate solvers. The exact Riemann solver is applied at all the cell interfaces every time step with a Newton–Raphson iterative scheme. This is one of the reasons why it has not been implemented as widely as the approximate solvers. As a result, an explicit analytical solver of the exact Riemann problem that does not require an iterative scheme will be of interest to many researchers in the field.

The present paper describes an alternate solution to the exact Riemann problem through the homotopy analysis method [19, 20]. The method has been applied to many nonlinear problems, such as the Blasius viscous flow [21, 22], boundary layer flows of non-Newtonian fluids [23],

DOI: 10.1002/fld

nonlinear water waves [24], generalized Hirota–Satsuma coupled KdV equation [25], thin film flows of a fourth-grade fluid [26], and even the valuation of American put options [27], and produced highly accurate numerical and analytical solutions to the governing partial different equations. In addition, it has been implemented with other numerical techniques such as the boundary element method for the solution of nonlinear problems [28, 29]. The following section provides a summary for the nonlinear shallow-water equations and the associated Riemann problem and describes the implementation of the homotopy analysis method to provide a series solution to the exact Riemann problem. This is followed by a description and a convergence analysis of the proposed Riemann solver for the two-shock and shock-rarefaction cases. The application of the Riemann solver in the nonlinear shallow-water equations is demonstrated through one and two-dimensional numerical examples to arrive at the conclusions and the recommendations for future work.

2. MATHEMATICAL FORMULATION

2.1. Riemann problem for shallow-water equations

The depth-integrated shallow-water equations include a continuity equation and two momentum equations in the horizontal plane. In the Cartesian (x, y) coordinate system, the conservative form of the nonlinear shallow-water equations is given by

$$\frac{\partial \mathbf{U}}{\partial t}+\frac{\partial \mathbf{F}}{\partial x}+\frac{\partial \mathbf{G}}{\partial y}=0 \tag{1}$$

where t denotes time, $\mathbf{U}$ is the vector of conserved variables, and $\mathbf{F}$ and $\mathbf{G}$ are the Cartesian components of the flux tensor. These vectors are expressed in terms of the flow depth h and the flow velocity (u, v) as

$$\mathbf{U}=\begin{bmatrix} h \\ uh \\ vh \end{bmatrix}, \quad \mathbf{F}=\begin{bmatrix} uh \\ u^2h+gh^2/2 \\ uvh \end{bmatrix} \quad \text{and} \quad \mathbf{G}=\begin{bmatrix} vh \\ uvh \\ v^2h+gh^2/2 \end{bmatrix} \tag{2}$$

where g is gravitational acceleration. The hyperbolic system of equations, which has three real and distinct eigenvalues, admit both continuous and discontinuous solutions. A Godunov-type scheme based on the solution of a local Riemann problem provides an effective approach to capture the pertinent flow characteristics.

Direct solutions are not available for two or higher-dimensional Riemann problems. A splitting technique reduces the problem into two one-dimensional problems. For the x-split component, the Riemann problem can be expressed as

$$\frac{\partial \mathbf{U}}{\partial t}+\frac{\partial \mathbf{F}}{\partial x}=0 \tag{3}$$

DOI: 10.1002/fld

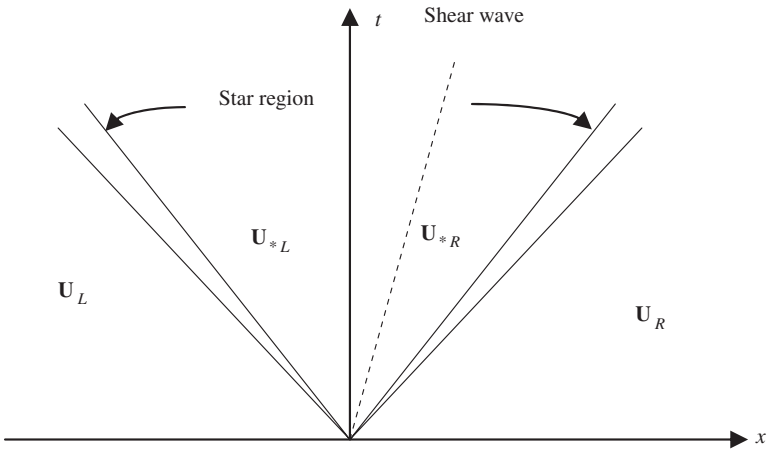

Figure 1. General solution of the Riemann problem with a wet bed.

with the initial state

$$\mathbf{U}(x,0)=\begin{cases}\mathbf{U}_{\mathrm{L}} & \text{if } x\leqslant 0\\ \mathbf{U}_{\mathrm{R}} & \text{if } x>0\end{cases} \tag{4}$$

where the subscripts L and R denote the left and right regions, respectively. This Riemann problem with an initial discontinuity at $x=0$ is a generalization of the dam-break problem. Figure 1 illustrates the solution, which consists of shock and rarefaction waves propagating from the discontinuity and separated by the shear wave. Between the left and right regions is the star region, in which the flow depth and velocity are determined from a Riemann solver.

The constancy of Riemann invariants across rarefaction waves and the Rankine–Hugoniot jump conditions across shock waves give rise to the following nonlinear algebraic equation for the flow depth h_* in the star region [30]:

$$f_{\mathrm{L}}(h_*,h_{\mathrm{L}})+f_{\mathrm{R}}(h_*,h_{\mathrm{R}})+\Delta u=0 \tag{5}$$

where

$$f_{\mathrm{L}}(h_*,h_{\mathrm{L}})=\begin{cases}2(\sqrt{gh_*}-\sqrt{gh_{\mathrm{L}}}), & h_*\leqslant h_{\mathrm{L}} \quad \text{(rarefaction)}\\ (h_*-h_{\mathrm{L}})\sqrt{\dfrac{1}{2}g\dfrac{h_*+h_{\mathrm{L}}}{h_*h_{\mathrm{L}}}}, & h_*>h_{\mathrm{L}} \quad \text{(shock)}\end{cases} \tag{6}$$

$$f_{\mathrm{R}}(h_*,h_{\mathrm{R}})=\begin{cases}2(\sqrt{gh_*}-\sqrt{gh_{\mathrm{R}}}), & h_*\leqslant h_{\mathrm{R}} \quad \text{(rarefaction)}\\ (h_*-h_{\mathrm{R}})\sqrt{\dfrac{1}{2}g\dfrac{h_*+h_{\mathrm{R}}}{h_*h_{\mathrm{R}}}}, & h_*>h_{\mathrm{R}} \quad \text{(shock)}\end{cases} \tag{7}$$

$$\Delta u=u_{\mathrm{R}}-u_{\mathrm{L}} \tag{8}$$

The solution of u_* follows directly as

$$u_*=\tfrac{1}{2}(u_{\mathrm{L}}+u_{\mathrm{R}})+\tfrac{1}{2}[f_{\mathrm{R}}(h_*,h_{\mathrm{R}})-f_{\mathrm{L}}(h_*,h_{\mathrm{L}})] \tag{9}$$

DOI: 10.1002/fld

Since there is no general close-form solution to the nonlinear algebraic equation (5), the *exact* solution is sought numerically by a Newton–Raphson iteration scheme:

$$h_*^{i+1} = h_*^i - \frac{f_L(h_*^i, h_L) + f_R(h_*^i, h_R) + \Delta u}{f'_L(h_*^i, h_L) + f'_R(h_*^i, h_R)} \tag{10}$$

where the superscripts indicate the result at the ith or $(i+1)$th iteration and the prime indicates a derivative with respect to h_*. The iterative scheme starts with an initial guess h_*^0 and continues until the change in h_* is smaller than a prescribed tolerance.

2.2. Homotopy analysis method

The homotopy analysis method described by Liao [19, 20] is an extension of the fundamental concept of topology for the solution of nonlinear differential equations. This analytic technique is based on a continuous variation from an initial approximation to the exact solution through a series of deformation equations. The method is adapted here to provide explicit solutions for the nonlinear algebraic equation (5), expressed in the form

$$\mathcal{N}[h_*] = 0 \tag{11}$$

where $\mathcal{N}$ is a nonlinear operator depending on the combination of shock and rarefaction waves. The solution is mapped to the function $H(q)$ such that, as the embedding parameter q increases from 0 to 1, $H(q)$ varies continuously from the initial approximation h_0 to the exact solution h_* through the zeroth-order deformation equation:

$$(1-q)\{\mathcal{F}[H(q)] - \mathcal{F}[h_0]\} = q\hbar\mathcal{N}[H(q)] \tag{12}$$

where $\mathcal{F}$ is an operator chosen to give $H(0) = h_0$ and $H(1) = h_*$ at the two limits of the variation and $\hbar \neq 0$ is an auxiliary parameter controlling the convergence rate and region of the solution. Through this auxiliary parameter, Equation (12) allows a large degree of freedom in the selection of the initial approximation h_0 and the operator $\mathcal{F}$ for rapid convergence of the solution.

When dealing with nonlinear differential equations, the operator $\mathcal{F}$ is usually a linearized version of the nonlinear operator $\mathcal{N}$ to facilitate reduction of the zeroth-order deformation equation into a series of linear equations [20–27]. This is, however, not a necessary condition for the solution of a nonlinear algebraic equation. By choosing $\mathcal{F} = \mathcal{N}$, we fully account for the nonlinear characteristics in the variation and speeds up the convergence toward the exact solution. This gives rise to the following zeroth-order deformation equation:

$$(1-q)\{\mathcal{N}[H(q)] - \mathcal{N}(h_0)\} = q\hbar\mathcal{N}[H(q)] \tag{13}$$

which represents a departure from the conventional homotopy analysis method. The variation to the exact solution is implemented through a successive approximation with the initial approximation as the first term. To this end, $H(q)$ is expanded in a Taylor series about $q = 0$ as

$$H(q) = h_0 + \sum_{m=1}^{\infty} h_m q^m \tag{14}$$

where

$$h_m = \frac{1}{m!}\frac{\mathrm{d}^m}{\mathrm{d}q^m} H(q)\bigg|_{q=0} \tag{15}$$

DOI: 10.1002/fld

If the initial approximation h_0 and the auxiliary parameter $\hbar$ are also properly chosen, the series (14) converges at $q=1$ to give the exact solution

$$h_* = \sum_{m=0}^{\infty} h_m \tag{16}$$

This expression provides a relationship between the initial approximation h_0 and the exact solution h_* by means of the higher-order terms h_m derived from Equation (15).

The derivative $\mathrm{d}^m H(q)/\mathrm{d}q^m$ in Equation (15) may be derived from the mth order deformation equation, which is obtained by differentiating Equation (13) m times with respective to the embedding parameter q:

$$\frac{\mathrm{d}^m}{\mathrm{d}q^m}\mathcal{N}[H(q)] = \frac{\mathrm{d}^{m-1}}{\mathrm{d}q^{m-1}}\left\{q(1+\hbar)\frac{\mathrm{d}}{\mathrm{d}q}\mathcal{N}[H(q)] + (1+\hbar)\mathcal{N}[H(q)] - \mathcal{N}(h_0)\right\} \quad \text{for } m \geqslant 1 \tag{17}$$

For $m=1$ and $q=0$, it follows straightforwardly from Equations (15) and (17) that

$$h_1 = \hbar\frac{\mathcal{N}(h_0)}{\mathcal{N}^{(1)}(h_0)} \tag{18}$$

where the superscript in parentheses indicates the order of derivative with respect to h_0. For $m \geqslant 2$, the derivatives of the composite function $\mathcal{N}[H(q)]$ are expanded by Faà di Bruno's formula to give an explicit expression for

$$\frac{\mathrm{d}^m H(q)}{\mathrm{d}q^m} = \left\{(1+\hbar)m\frac{\mathrm{d}^{m-1}}{\mathrm{d}q^{m-1}}\mathcal{N}[H(q)] + q\frac{\mathrm{d}^m}{\mathrm{d}q^m}\mathcal{N}[H(q)] - \sum_{k=2}^{m}\frac{\mathrm{d}^k\mathcal{N}(H)}{\mathrm{d}H^k} \times B_{m,k}\left[\frac{\mathrm{d}H(q)}{\mathrm{d}q}, \frac{\mathrm{d}^2H(q)}{\mathrm{d}q^2}, \ldots, \frac{\mathrm{d}^{m-k+1}H(q)}{\mathrm{d}q^{m-k+1}}\right]\right\}\left(\frac{\mathrm{d}\mathcal{N}}{\mathrm{d}H}\right)^{-1} \quad \text{for } m \geqslant 2 \tag{19}$$

in which $B_{m,k}$ denotes the Bell polynomials given by

$$B_{m,k}\left[\frac{\mathrm{d}H(q)}{\mathrm{d}q}, \frac{\mathrm{d}^2H(q)}{\mathrm{d}q^2}, \ldots, \frac{\mathrm{d}^{m-k+1}H(q)}{\mathrm{d}q^{m-k+1}}\right] = \sum \frac{m!}{j_1!j_2!\ldots j_{m-k+1}!}\left(\frac{\mathrm{d}H(q)}{1!\mathrm{d}q}\right)^{j_1}\left(\frac{\mathrm{d}^2H(q)}{2!\mathrm{d}q^2}\right)^{j_2}\cdots\left(\frac{\mathrm{d}^{m-k+1}H(q)}{(m-k+1)!\mathrm{d}q^{m-k+1}}\right)^{j_{m-k+1}} \tag{20}$$

where the summation is over all nonnegative integers $j_1, j_2, \ldots, j_{m-k+1}$ for which $j_1+j_2+\cdots+j_{m-k+1}=k$ and $j_1+2j_2+\cdots+(m-k+1)j_{m-k+1}=m$ [31]. With $q=0$, Equation (19) gives rise to the second and higher-order terms of Equation (15) as

$$h_m = \frac{(1+\hbar)}{(m-1)!\mathcal{N}^{(1)}(h_0)}\sum_{k=1}^{m-1}\mathcal{N}^{(k)}(h_0)B_{m-1,k}[h_1, 2h_2, \ldots, (m-k)!h_{m-k}] - \frac{1}{m!\mathcal{N}^{(1)}(h_0)}\sum_{k=2}^{m}\mathcal{N}^{(k)}(h_0)B_{m,k}[h_1, 2h_2, \ldots, (m-k+1)!h_{m-k+1}] \quad \text{for } m \geqslant 2 \tag{21}$$

DOI: 10.1002/fld

Equation (21) provides a recursive formula to determine the mth order term from the first $(m-1)$ terms of the series.

Both Equations (18) and (21) do not contain the embedding parameter q. The solution to the Riemann problem can be expressed explicitly in terms of the nonlinear operator in Equation (5) and the initial approximation h_0 as

$$h_* = h_0 + \hbar \frac{\mathcal{N}(h_0)}{\mathcal{N}^{(1)}(h_0)} + \sum_{m=2}^{\infty} \left(\frac{(1+\hbar)}{(m-1)!\mathcal{N}^{(1)}(h_0)} \sum_{k=1}^{m-1} \mathcal{N}^{(k)}(h_0) B_{m-1,k}[h_1, 2h_2, \ldots, (m-k)!h_{m-k}] \right.$$

$$\left. - \frac{1}{m!\mathcal{N}^{(1)}(h_0)} \sum_{k=2}^{m} \mathcal{N}^{(k)}(h_0) B_{m,k}[h_1, 2h_2, \ldots, (m-k+1)!h_{m-k+1}] \right) \tag{22}$$

Since the Taylor series (14) is unique, its convergence will lead to the exact solution in Equation (22). If we take the first-order approximation with $\hbar = -1$, Equation (22) becomes

$$h_* = h_0 - \frac{\mathcal{N}(h_0)}{\mathcal{N}^{(1)}(h_0)} \tag{23}$$

which is equivalent to the first iteration of the Newton–Raphson scheme in Equation (10). At higher orders, the homotopy analysis method provides a continuous refinement of the initial approximation instead of functioning as an iterative scheme. It also provides a mechanism to optimize the convergence rate and region of the solution through the auxiliary parameter $\hbar$. Equation (22) also presents a general series solution for nonlinear algebraic equations of a single unknown variable. In spite of its appearance, the expression is rather simple in symbolic computation and is ready for general application.

3. RIEMANN SOLVER FOR SHALLOW-WATER EQUATIONS

There are three possible cases for the solution of the Riemann problem. These correspond to two rarefaction waves, two-shock waves, and one rarefaction and one shock wave on the opposite sides of the discontinuity. For the case of two rarefaction waves, the constancy of the Riemann invariants and the monotonic variation of the eigenvalues indicate that the solution is limited to $h_* \leqslant h_{\mathrm{L}}$ and $h_* \leqslant h_{\mathrm{R}}$. The initial state must satisfy the following condition derived from Equation (5):

$$2(\sqrt{gh_{\mathrm{L}}} + \sqrt{gh_{\mathrm{R}}}) > \Delta u \geqslant 2|\sqrt{gh_{\mathrm{L}}} - \sqrt{gh_{\mathrm{R}}}| \tag{24}$$

The close-form solution in the star region is given by

$$h_* = \frac{1}{g}\left[\frac{1}{2}(\sqrt{gh_{\mathrm{L}}} + \sqrt{gh_{\mathrm{R}}}) - \frac{1}{4}\Delta u\right]^2 \tag{25}$$

$$u_* = \tfrac{1}{2}(u_{\mathrm{L}} + u_{\mathrm{R}}) + \sqrt{gh_{\mathrm{L}}} - \sqrt{gh_{\mathrm{R}}} \tag{26}$$

There is, however, no close-form solution for the cases of two-shock waves and shock-rarefaction waves. In this section, we derive explicit solutions for these two cases from the general series solution in Equation (22). Careful selections of the initial approximation and auxiliary parameter ensure a fast converging series with a finite number of terms to allow implementation of the solver in existing numerical models.

DOI: 10.1002/fld

3.1. Two shock waves solution

Based on the Rankine–Hugoniot conditions and the entropy condition, the solution for the case of two-shock waves correspond to $h_*>h_L$ and $h_*>h_R$. Equation (5) gives rise to the following condition for the initial state:

$$\Delta u<-|h_L-h_R|\sqrt{\frac{1}{2}g\frac{h_L+h_R}{h_Lh_R}} \tag{27}$$

The nonlinear algebraic equation (5) becomes

$$(h_*-h_L)\sqrt{\frac{1}{2}g\frac{h_*+h_L}{h_*h_L}}+(h_*-h_R)\sqrt{\frac{1}{2}g\frac{h_*+h_R}{h_*h_R}}+\Delta u=0 \tag{28}$$

which defines the nonlinear operator in the series solution (22). Although this is not a requirement, a linear solution of the nonlinear problem is typically used as the initial approximation in the homotopy analysis method [19–27]. We follow this approach and choose the initial approximation

$$h_0=\frac{-\sqrt{h_Lh_R/g}\Delta u+h_L\sqrt{h_R}+h_R\sqrt{h_L}}{\sqrt{h_L}+\sqrt{h_R}} \tag{29}$$

which is the solution of the linearized Equation (28) in the form

$$(h_*-h_L)\sqrt{\frac{g}{h_L}}+(h_*-h_R)\sqrt{\frac{g}{h_R}}+\Delta u=0 \tag{30}$$

While other linearized versions of Equation (28) exist, the use of the solution of Equation (30), albeit other factors, results in the most rapid convergence of the series solution (22).

Equation (22) may readily provide the solution in terms of the nonlinear operator and initial approximation defined by Equations (28) and (29), respectively. The series still contains the auxiliary parameter $\hbar$, which results in a family of solutions with varying convergence rates and regions. As pointed out by Liao [19, 20], there are always regions of $\hbar$ for convergence of the solutions. For a given nonlinear equation, the valid regions of $\hbar$ remain nearly the same for different values of the coefficients and must be determined through numerical experiments. Figure 2 plots the so-called $\hbar$-curves from two of the numerical experiments. The solution exhibits two distinct convergence patterns divided at approximately $\hbar=-1$, where the convergence rate is the most rapid. The first-order solution is a linear function of $\hbar$ and gives a reasonable approximation of the solution at $\hbar=-1$. Because Equation (21) is recursive, the higher-order solution is in the form of a polynomial of $\hbar$ to the same order. The numerical experiments indicate that the first three terms provide a highly accurate solution over $-1.1<\hbar<-0.9$ for possible ranges of initial states in the Riemann problem. Increasing the number of terms beyond the third order only serves to increase the convergence region with little influence on the accuracy of the solution.

The auxiliary parameter $\hbar$ is an important feature of the homotopy analysis method. It allows a careful examination of the convergence rate and region before a solver is proposed for the Riemann problem. By choosing $\hbar=-1$ and retaining the first three terms, we have the following solution for the flow depth in the star region under the condition defined by Equation (27):

$$h_*=\sum_{i=0}^{3}h_i \tag{31}$$

DOI: 10.1002/fld

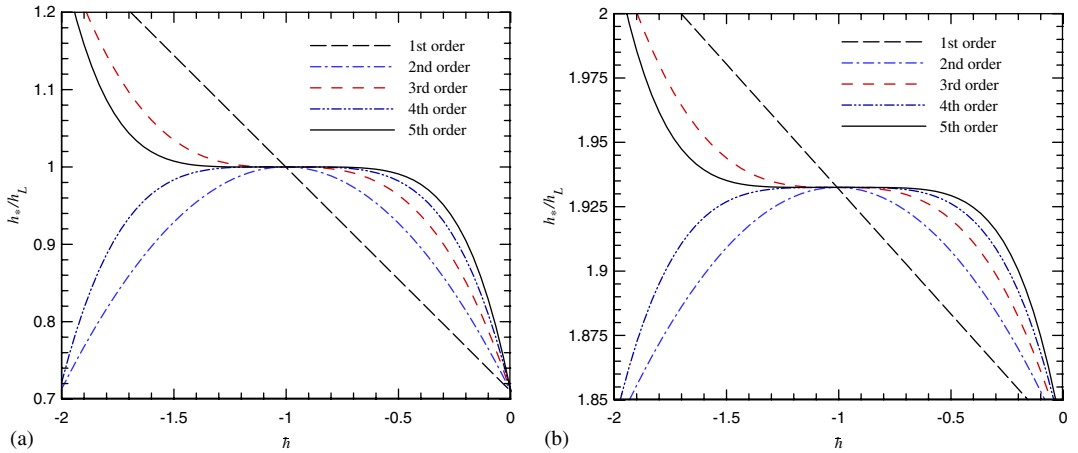

Figure 2. Convergence of the two shock waves solution with respect to the auxiliary parameter $\hbar$: (a) $\Delta u/\sqrt{gh_L/2}=-100$ and $h_R/h_L=0.0001$ and (b) $\Delta u/\sqrt{gh_L/2}=-2$ and $h_R/h_L=1.2$.

in which

$$h_1=\frac{-\Delta u\sqrt{2/g}+\alpha(h_L-h_0)+\beta(h_R-h_0)}{(h_L-h_0)/(2\alpha h_0^2)+(h_R-h_0)/(2\beta h_0^2)+\alpha+\beta} \tag{32}$$

$$h_2=\frac{h_1^2}{4\alpha^2\beta^2h_0^2}\frac{\alpha^3(5h_0+3h_R)+\beta^3(5h_0+3h_L)}{[2\alpha\beta h_0^2(\alpha+\beta)-h_0(\alpha+\beta)+(\beta h_L+\alpha h_R)]} \tag{33}$$

$$h_3=\frac{2h_2^2}{h_1}-\frac{h_1^3}{8\phi^2\psi^2h_0^2} \times\frac{\alpha\psi^3(\phi-1)[(5\phi^2+2\phi+1)h_L+h_0(\phi^2-1)]+\beta\phi^3(\psi-1)[(5\psi^2+2\psi+1)h_R+h_0(\psi^2-1)]}{\alpha\psi(\phi-1)h_L+\beta\phi(\psi-1)h_R+\alpha\psi(\phi+1)h_0+\beta\phi(\psi+1)h_0} \tag{34}$$

where

$$\alpha=\sqrt{\frac{1}{h_L}+\frac{1}{h_0}},\quad \beta=\sqrt{\frac{1}{h_R}+\frac{1}{h_0}},\quad \phi=1+\frac{h_L}{h_0},\quad \psi=1+\frac{h_R}{h_0} \tag{35}$$

The flow velocity in the star region follows as

$$u_*=\frac{1}{2}(u_L+u_R)+\frac{1}{2}\sqrt{\frac{g}{2}}\left[(h_*-h_R)\sqrt{\frac{h_*+h_R}{h_*h_R}}-(h_*-h_L)\sqrt{\frac{h_*+h_L}{h_*h_L}}\right] \tag{36}$$

Figure 3 compares the proposed Riemann solver with the exact solver determined by the Newton–Raphson iterative scheme. The results show rapid convergence of the proposed Riemann solver

DOI: 10.1002/fld

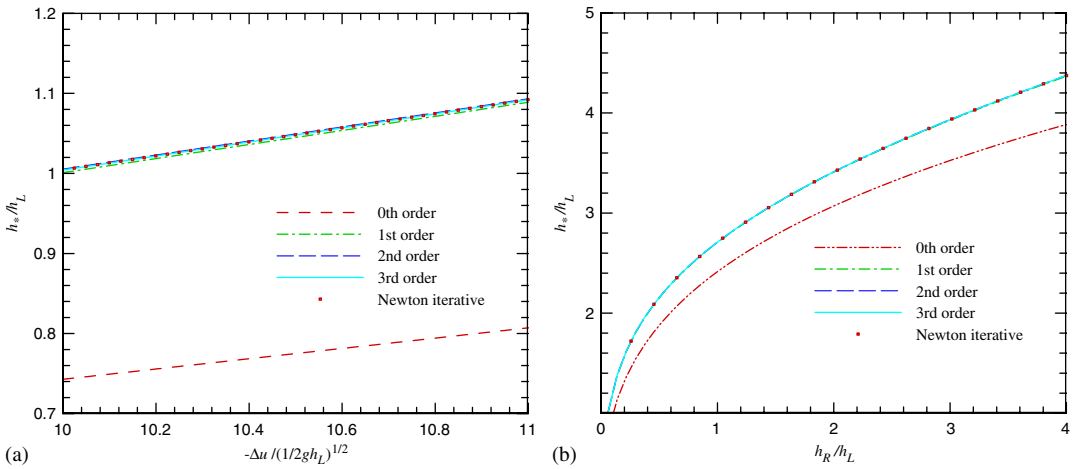

Figure 3. Convergence of the solution for two shock waves: (a) over velocity difference for $h_R/h_L=0.01$ and (b) over flow depth difference for $\Delta u/\sqrt{gh_L/2}=-4$.

over wide ranges of depth and velocity discontinuities. The first-order solution provides a very good approximation, while the second and third-order solutions are almost identical to the exact Riemann solver.

3.2. *One shock wave and one rarefaction wave solution*

For demonstration, we consider the case of a shock wave on the left and a rarefaction wave on the right. The Rankine–Hugoniot jump conditions indicate that no shock waves can be adjacent to a region of dry bed giving rise to $h_L>0$ and $h_R\geqslant 0$. The nonlinear algebraic equation (5) becomes

$$(h_*-h_L)\sqrt{\frac{h_*+h_L}{h_*h_L}}+2\sqrt{2}(\sqrt{h_*}-\sqrt{h_R})+\sqrt{\frac{2}{g}}\Delta u=0 \tag{37}$$

where $h_*>h_L$ and $h_R\geqslant h_*$. From Equation (5), the initial state must satisfy

$$2(\sqrt{gh_R}-\sqrt{gh_L})>\Delta u\geqslant(h_L-h_R)\sqrt{\frac{1}{2}g\frac{h_L+h_R}{h_Lh_R}} \quad \text{and} \quad h_R>h_L \tag{38}$$

It is straightforward to choose the initial approximation

$$h_0=h_L+\sqrt{\frac{2h_Lh_R}{g(h_L+h_R)}}[-\Delta u+2\sqrt{g}(\sqrt{h_R}-\sqrt{h_L})] \tag{39}$$

This is the solution of the linearized Equation (37) in the form

$$(h_*-h_L)\sqrt{\frac{h_R+h_L}{h_Rh_L}}+2\sqrt{2}(\sqrt{h_L}-\sqrt{h_R})+\sqrt{\frac{2}{g}}\Delta u=0 \tag{40}$$

DOI: 10.1002/fld

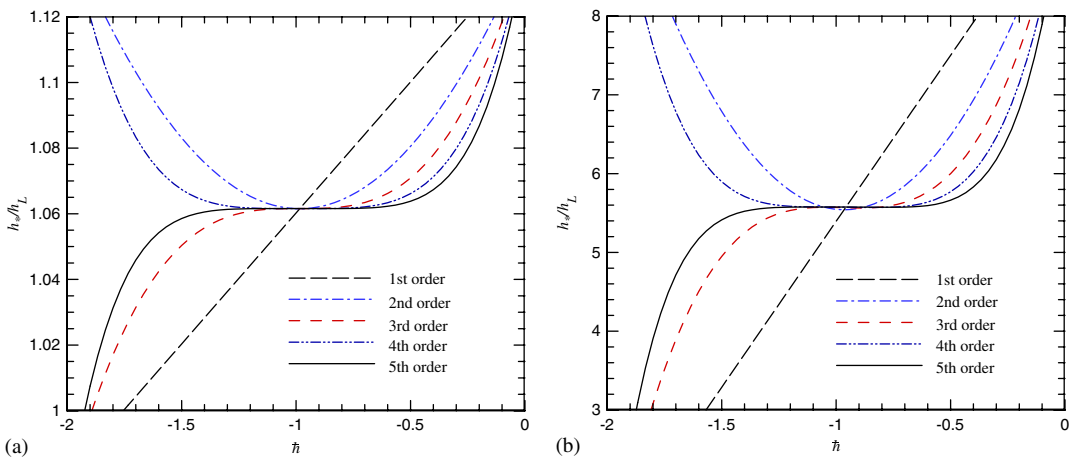

Figure 4. Convergence of the shock-rarefaction solution with respect to the auxiliary parameter $\hbar$: (a) $\Delta u/\sqrt{gh_L/2}=1$ and $h_R/h_L=2$ and (b) $\Delta u/\sqrt{gh_L/2}=1$ and $h_R/h_L=20$.

that gives the most rapid convergence among other possible alternatives. Equations (37) and (39), respectively, provide the nonlinear operator and initial approximation to the solution series in Equation (22). A numerical experiment indicates that the solution converges most rapidly around $\hbar=-1$. The convergence pattern shown in Figure 4 is similar to the case of two-shock waves as it is determined by the overall structure of the series solution (22). The results show an increasing convergence region with increasing number of terms. The third-order solution is sufficient for most practical application with a valid range of $-1.1<\hbar<-0.9$.

By choosing $\hbar=-1$ and retaining the first three terms, we have the following solution for the flow depth in the star region under the condition defined by Equation (38):

$$h_*=\sum_{i=0}^{3}h_i \tag{41}$$

in which

$$h_1=-\frac{2\alpha h_L h_0^2(h_0\alpha-\alpha h_L+\Delta u\sqrt{2/g}-2\sqrt{2h_R}+2\sqrt{2h_0})}{2h_0^2+2\sqrt{2}\alpha h_L h_0^{3/2}+h_0h_L+h_L^2} \tag{42}$$

$$h_2=\frac{h_0(\phi-1)^2+h_L(3\phi^2+2\sqrt{2h_0}\alpha\phi-2\phi-1)}{4\phi h_0[h_0(\phi+1)+h_L(\phi+2\sqrt{2h_0}\alpha-1)]}h_1^2 \tag{43}$$

$$h_3=\frac{2h_2^2}{h_1}-\frac{h_L(5\phi^3+2\sqrt{2h_0}\alpha\phi^2-3\phi^2-\phi-1)+h_0(\phi-1)^2(\phi+1)}{8\phi^2h_0^2[h_0(\phi+1)+h_L(\phi+2\sqrt{2h_0}\alpha-1)]}h_1^3 \tag{44}$$

The flow velocity in the star region follows as

$$u_*=\frac{1}{2}(u_L+u_R)+\frac{1}{2}\left[2(\sqrt{gh_*}-\sqrt{gh_R})-(h_*-h_L)\sqrt{\frac{1}{2}g\frac{h_*+h_L}{h_*h_L}}\right] \tag{45}$$

DOI: 10.1002/fld

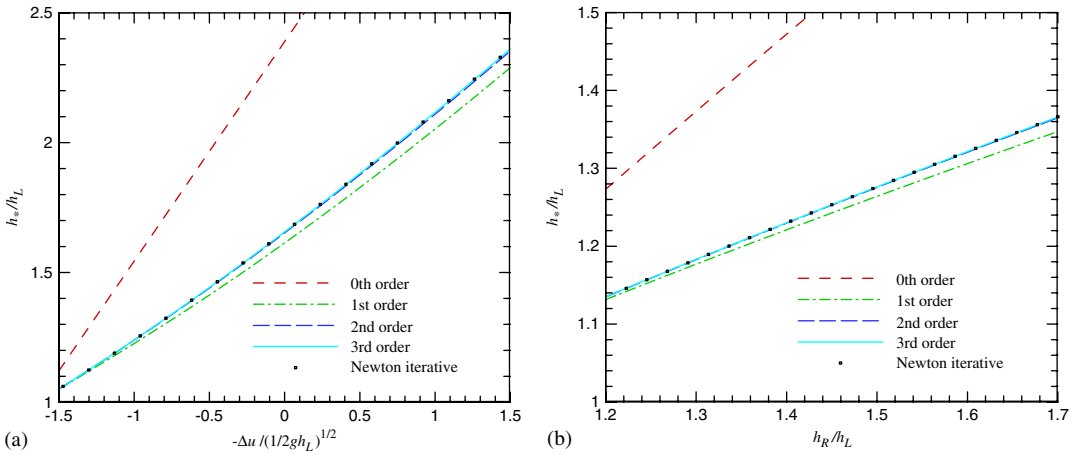

Figure 5. Convergence of the solution for one shock wave and one rarefaction wave: (a) over velocity difference for $h_R/h_L=2.5$ and (b) over flow depth difference for $\Delta u/\sqrt{gh_L/2}=-0.1$.

Figure 5 shows comparisons of the solution with that obtained by the Newton–Raphson iterative scheme over ranges of initial states. The first-order solution represents a major improvement over the initial approximation. Rapid convergence occurs at second order, and the third-order solution is sufficient for general application of the solver. The solution for the case of a rarefaction wave on the left and a shock wave on the right can be obtained from Equation (41) to (45) by reversing the flow depths on the left and right sides.

4. NUMERICAL EXAMPLES

The Riemann solver is an important component of the Godunov-type schemes for the nonlinear shallow-water equations. The proposed Riemann solver is simple and explicit and thus can easily be implemented into existing finite-volume models. As a demonstration, we use the two-dimensional finite-volume model of Wei *et al.* [17] to examine the implementation of the proposed Riemann solver. The model uses uniform rectangular cells with dimensions $(\Delta x,\ \Delta y)$ in a Cartesian grid and integrates the governing equations with a time-step size Δt. Equation (1) becomes

$$\mathbf{U}_{i,j}^{k+1}=\mathbf{U}_{i,j}^{k}-\frac{\Delta t}{\Delta x}(\mathbf{F}_{i+1/2,j}^{k+1/2}-\mathbf{F}_{i-1/2,j}^{k+1/2})-\frac{\Delta t}{\Delta y}(\mathbf{G}_{i,j+1/2}^{k+1/2}-\mathbf{G}_{i,j-1/2}^{k+1/2}) \tag{46}$$

where k denotes the current time step and (i, j) denote indices at the cell centroid. The vectors $\mathbf{U}_{i,j}^{k}$ and $\mathbf{U}_{i,j}^{k+1}$ represent the cell averages at the respective time steps. Equation (46) poses a series of local Riemann problems at the cell interfaces, where the flux vectors $\mathbf{F}_{i\pm1/2,j}$ and $\mathbf{G}_{i,j\pm1/2}$ are evaluated from the Riemann solver. The model uses an explicit second-order splitting scheme for the time integration and achieves a second-order accuracy in space through a piecewise linear interpolation of the conserved variables with the van-Leer limiter.

DOI: 10.1002/fld

4.1. One-dimensional dam-break problems

The finite-volume model with the proposed Riemann solver is first verified with one-dimensional shallow-water problems involving flow discontinuities that mimic the Riemann problem itself. Toro [30] describes a series of numerical examples to demonstrate the Godunov-type schemes for shock capturing. Each of these examples was designed to present a particular degree of difficulty for the testing of numerical methods. Two of the examples involving shock and rarefaction waves and two-shock waves are considered here to examine the implementation of the proposed Riemann solver.

The first example corresponds to a generalized dam-break problem in a 50 m long channel. The dam is located at 10 m from the left boundary. The initial flow depth and velocity are respectively 1.0 m and 2.5 m/s in the left region and 0.1 m and 0 m/s on the right. The cell width $\Delta x = 0.5$ m and time step $\Delta t = 0.01$ s are selected to satisfy the Courant criterion. The dam is removed instantly at $t = 0$. Figure 6 shows the flow depth and velocity along the channel at $t = 7$ s. The results show a critical left-propagating rarefaction wave and a strong right-propagating shock wave. Between the rarefaction wave and shock wave is the star region with constant flow depth and velocity. The model with the proposed Riemann solver accurately captures the propagation of the shock wave and the development of the rarefaction fan. The computed flow depth and velocity give very good agreement with the exact solution provided by Toro [30] based on a Newton–Raphson scheme.

The second numerical example corresponds to the shock waves generated by a discontinuity of the flow velocity in the channel. At $t = 0$, the water depth along the channel is constant at 1.0 m and the flow discontinuity is located at $x = 20$ m. The flow velocity is 1.5 m/s on the left and the water is at rest on the right of the discontinuity. The computation is based on $\Delta x = 0.5$ m and $\Delta t = 0.01$ s. The discontinuity generates two-shock waves propagating in the opposite directions. Figure 7 shows the flow depth and velocity associated with the shock waves at $t = 6$ s. The model correctly captures the propagation speed, the strength of the jump, and the width of the shock layer. The computed flow depth and velocity are free of spurious oscillations associated with shock waves.

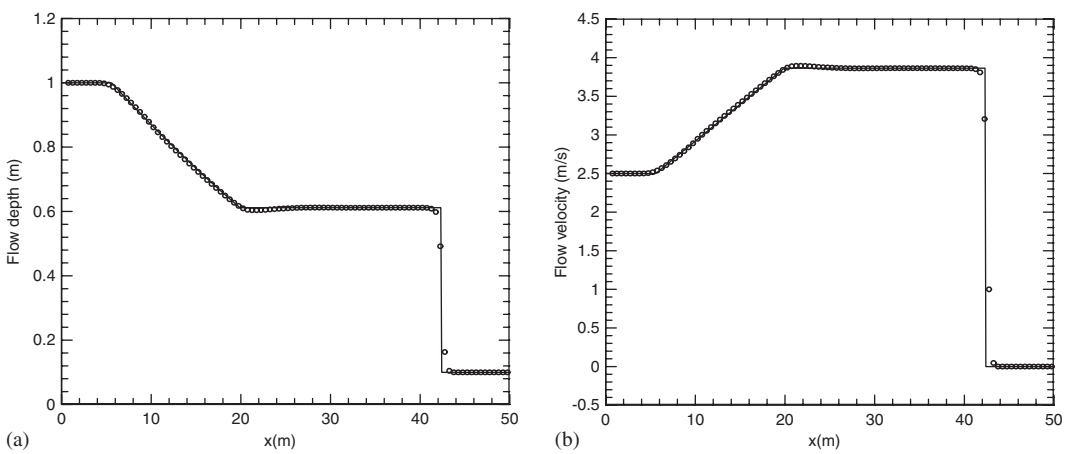

Figure 6. Comparison of the present numerical solution (symbol) and the exact solution (line) at $t = 7$ s for $h_L = 1.0$ m, $h_R = 0.1$ m, $u_L = 2.5$ m/s, and $u_R = 0.0$ m/s: (a) flow depth and (b) flow velocity.

DOI: 10.1002/fld

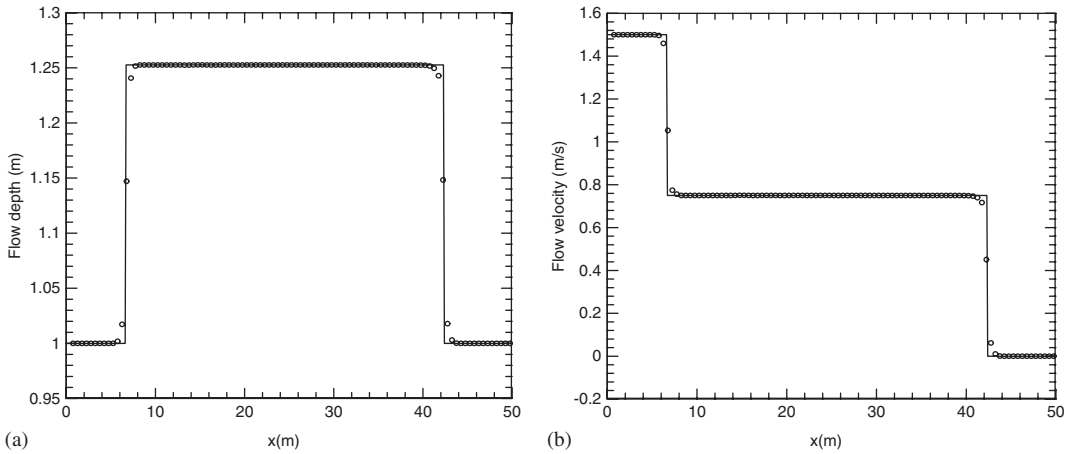

Figure 7. Comparison of the present numerical solution (symbol) and the exact solution (line) at $t=6$ s for $h_L=1.0$ m, $h_R=1.0$ m, $u_L=1.5$ m/s, and $u_R=0.0$ m/s: (a) flow depth and (b) flow velocity.

The results from this example show excellent agreement with the exact solution, together with the test case above, illustrating the accuracy of the proposed Riemann solver for implementation in a finite-volume model.

4.2. Two-dimensional dam-break problem

The circular dam-break problem of Toro [30] provides a demanding test case for the implementation of the proposed Riemann solver in two-dimensional finite-volume models. The dam, which is an infinitesimally thin circular wall with a radius of 2.5 m, is located at the center of a square computational domain of $40\,\text{m}\times 40\,\text{m}$. The water levels inside and outside the dam are 2.5 and 0.5 m, respectively. The circular wall is removed instantly at $t=0$ s and the subsequent evolution of the wave pattern and flow field in time is examined. This numerical example has some very clear discontinuous features for model testing. Liang *et al.* [32] investigate this problem for verification of a model based on the HLLC solver and dynamically adaptive quadtree grids. Similar problems with different initial states have also been studied by Alcrudo and Garcia-Navarro [33], Billett and Toro [34], and Mingham and Causon [35].

The computation uses a cell width of 0.1 m in both the x and y directions and a time step of $\Delta t=0.005$ s. The circular water column at the initial state is approximated by square cells, resulting in a jagged circumference. The water depth of a cell cut across by the circular wall is assigned a value based on the weighted average of the cell areas inside and outside the wall. Figure 8 shows three-dimensional perspective views of the initial surface elevation as well as the sequence of shock and rarefaction waves developed in the domain. Figure 9 provides the cross-sections of the flow depth and velocity at $t=0, 0.4$, and 0.7 s. The collapse of the dam generates an outward-propagating circular shock wave and a converging rarefaction wave. Different from one-dimensional dam-break problems, a depth gradient develops behind the shock wave. The rarefaction wave reaches the center at about $t=0.4$ s. The implosion of the water column and reflection of the rarefaction wave generate a very distinct dip of the surface elevation at the center.

DOI: 10.1002/fld

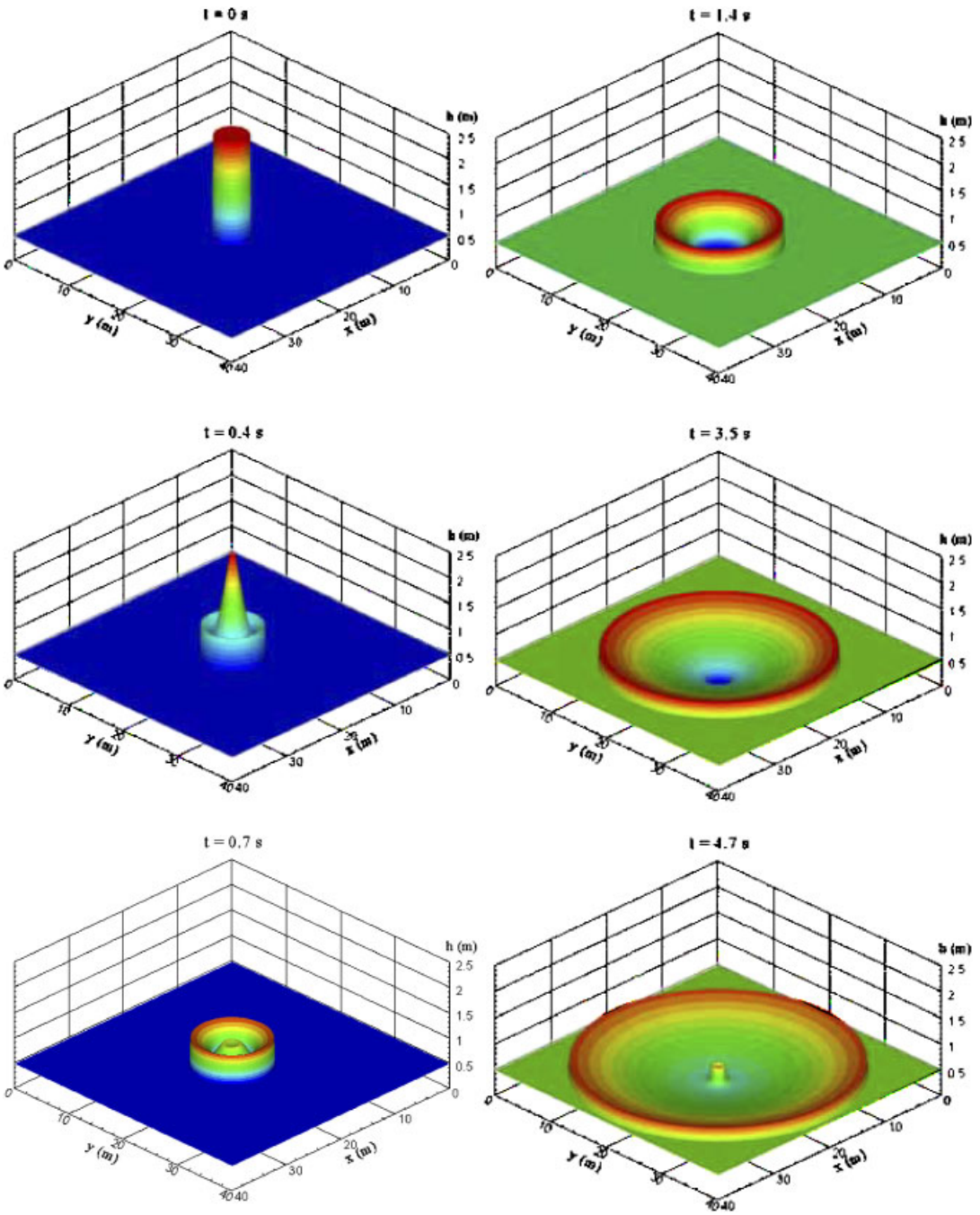

Figure 8. Perspective views of water surface after collapse of the circular dam.

DOI: 10.1002/fld

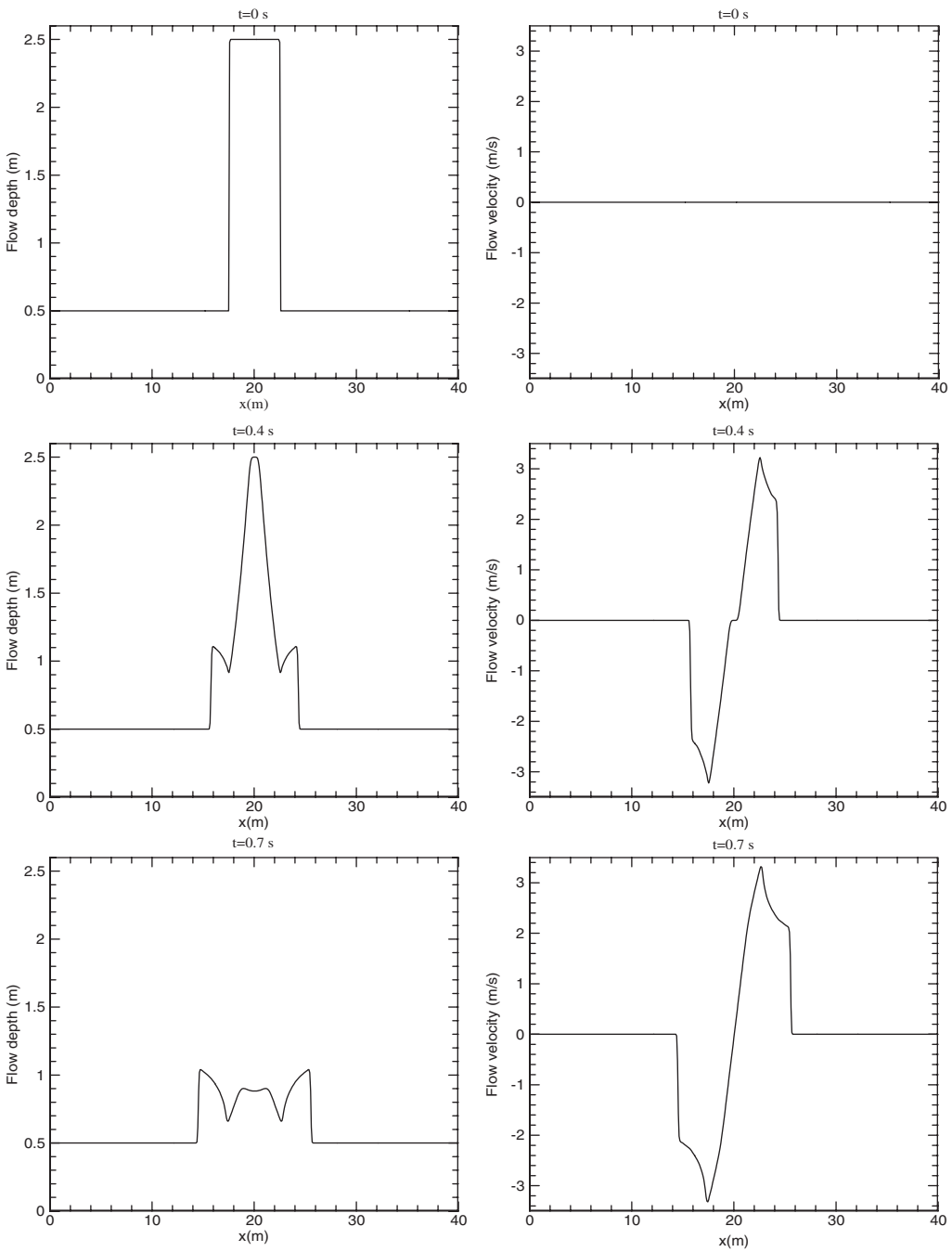

Figure 9. Profiles of flow depth and velocity along $y = 20\,\text{m}$ at $t = 0, 0.4$, and $0.7\,\text{s}$ after collapse of the circular dam.

DOI: 10.1002/fld

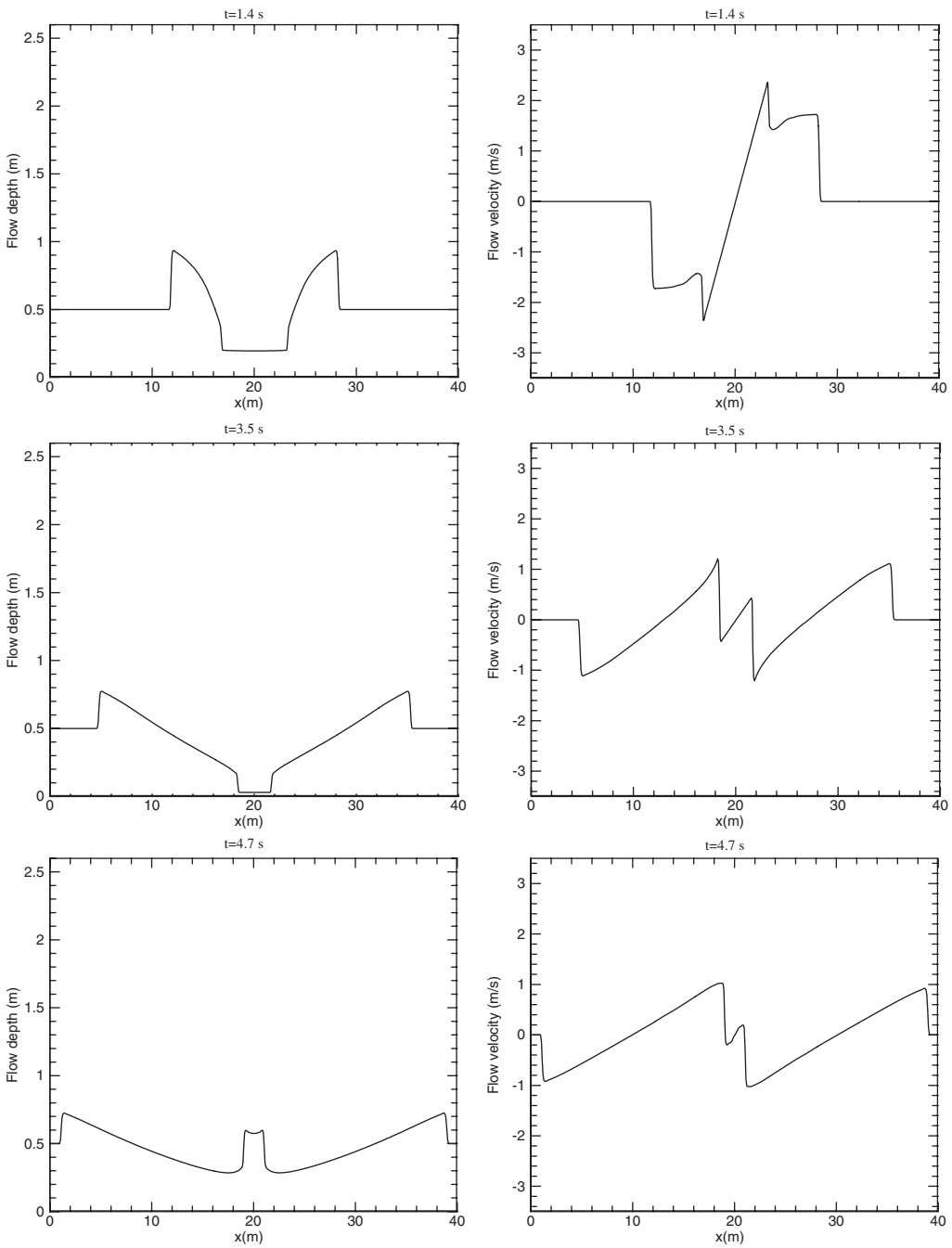

Figure 10. Profiles of flow depth and velocity along $y = 20\,\text{m}$ at $t = 1.4, 3.5$, and $4.7\,\text{s}$ after collapse of the circular dam.

DOI: 10.1002/fld

A new flow pattern develops as the dip expands outward and the water surface at the center falls below the outside water level of 0.5 m. Figure 10 provides the cross-sections of the flow depth and velocity at $t=1.4, 3.5$, and 4.7 s. A secondary shock was developed by $t=1.4$ s. The surface elevation near the center decreases sharply as this secondary shock propagates inward, while the outside shock wave continues to propagate outward with decreasing strength. The flow depth inside is very close to zero at $t=3.5$ s. The water surface jumps sharply when the secondary shock wave converges at the center and the reflection generates a third shock wave. As this shock wave propagates outward, a depth gradient develops behind the discontinuity resulting in another slight dip at the center. The calculation stops at $t=4.7$ s, when the outside shock wave is about to reach the boundary.

Despite the use of rectangular grids, the cylindrical symmetry of the shock and rarefaction waves is well maintained throughout the entire process as depicted in Figure 8. The propagation of the circular shock waves across the rectangular gridwork does not generate noticeable distortion to the surface. The approximation of the initial circular water column by square cells only results in minor modulation of the water surface in the circumferential direction. The modulation, which is most obvious in the surface plot at $t=0.4$ s, attenuates as the shock propagates outward. The finite-volume model accurately describes the dips and spikes of the surface elevation, which are right at the center of the domain and are difficult to resolve numerically. The sequence of shock and rarefaction waves, as well as their amplitudes, agrees very well with those reported by Toro [30], confirming the validity of the proposed Riemann solver over a wide parameter space.

5. CONCLUSIONS AND RECOMMENDATIONS

This paper describes the development and verification of an explicit solution to the exact Riemann problem of the nonlinear shallow-water equations. The homotopy analysis method provides a general series solution to the nonlinear algebraic equation resulting from the Riemann problem. Proper construction of the deformation equations and careful selection of the initial approximation and the auxiliary parameter result in rapid convergence of the solution series. The first three terms of the series provide a highly accurate Riemann solver for the cases of two-shock waves and shock-rarefaction waves.

The proposed solver is implemented in a finite-volume model with the Godunov-type scheme for demonstration and verification. The model produces excellent agreement of the shock and rarefaction waves with the exact solutions in two one-dimensional numerical examples. A two-dimensional benchmark example of the circular dam-break problem involving complex flow patterns further highlights the accuracy of the proposed Riemann solver over a large parameter space. The proposed Riemann solver is explicit and straightforward, and thus provides a useful alternative to approximate and numerical solvers in existing finite-volume models for long-wave calculations.

The present study also demonstrates the effectiveness of the homotopy analysis method in deriving explicit solutions for nonlinear algebraic equations. Many Riemann problems are cast in the form of nonlinear algebraic equations in terms of a single unknown that do not have close-form solutions. The proposed general series solution may provide explicit solutions to the generalized Riemann problem as well as the Riemann problem in two-phase and relativistic flows [36–38]. The proposed method also has applications in other numerical methods involving Riemann solvers, such as the smoothed particle hydrodynamics method and the discontinuous Galerkin finite element method.

DOI: 10.1002/fld

ACKNOWLEDGEMENTS

The research work reported in this paper is supported by the Office of Naval Research through Grant No. N00014-02-1-0903. SOEST Contribution Number 7201.

REFERENCES

1. Roe P. Approximate Riemann solvers, parameter vectors, and difference schemes. *Journal of Computational Physics* 1981; **43**(2):357–372.
2. Harten A, Hyman JM. Self adjusting grid methods for one-dimensional hyperbolic conservation laws. *Journal of Computational Physics* 1983; **50**(2):235–269.
3. Glaister P. Approximate Riemann solutions of the shallow water equations. *Journal of Hydraulic Research* 1988; **26**(3):293–306.
4. Dodd N. Numerical model of wave run-up, overtopping, and regeneration. *Journal of Waterway*, *Port*, *Coastal*, *and Ocean Engineering* 1998; **124**(2):73–81.
5. Hubbard ME, Dodd N. A 2D numerical model of wave run-up and overtopping. *Coastal Engineering* 2002; **47**(1):1–26.
6. Bradford SF, Sanders BF. Finite-volume model for shallow-water flooding of arbitrary topography. *Journal of Hydraulic Engineering* 2002; **128**(3):289–298.
7. LeVeque RJ. Balancing source terms and flux gradients in high-resolution Godunov methods: the quasi-steady wave-propagation algorithm. *Journal of Computational Physics* 1998; **146**(1):346–365.
8. Rossmanith JA, Bale DS, LeVeque RJ. A wave propagation algorithm for hyperbolic systems on curved manifolds. *Journal of Computational Physics* 2004; **199**(2):631–662.
9. Osher S, Solomon F. Upwind difference schemes for hyperbolic conservation laws. *Mathematics and Computation* 1982; **38**(158):229–374.
10. Zhao DH, Shen HW, Tabios III GQ, Lai JS, Tan WY. A finite-volume two-dimensional unsteady-flow model for river basins. *Journal of Hydraulic Engineering* 1994; **120**(7):863–883.
11. Harten A, Lax PD, van Leer B. On upstream differencing and Godunov-type schemes for hyperbolic conservation laws. *SIAM Review* 1983; **25**(1):35–61.
12. Einfeldt B. On Godunov-type methods for gas dynamics. *SIAM Journal on Numerical Analysis* 1988; **25**(2): 294–318.
13. Toro EF, Spruce M, Speares W. Restoration of the contact surface in the HLL-Riemann solver. *Shock Waves* 1994; **4**(1):25–34.
14. Hu K, Mingham CG, Causon DM. Numerical simulation of wave overtopping of coastal structures using the non-linear shallow water equations. *Coastal Engineering* 2000; **41**(4):433–465.
15. Zhou JG, Causon DM, Mingham CG, Ingram DM. The surface gradient method for the treatment of source terms shallow-water equations. *Journal of Computational Physics* 2001; **168**(1):1–25.
16. Brocchini M, Bernetti R, Mancinelli A, Albertini G. An efficient solver for nearshore flows based on the WAF method. *Coastal Engineering* 2001; **43**(2):105–129.
17. Wei Y, Mao XZ, Cheung KF. Well-balanced finite-volume model for long-wave runup. *Journal of Waterway*, *Port*, *Coastal*, *and Ocean Engineering* 2006; **132**(2):114–124.
18. Pan CH, Lin BY, Mao XZ. Case study: numerical modeling of the tidal bore on the Qiantang River, China. *Journal of Hydraulic Engineering* 2007; **133**(2):130–138.
19. Liao SJ. *Beyond Perturbation*: *Introduction to the Homotopy Analysis Method*. Chapman & Hall/CRC Press: Boca Raton, FL, 2003.
20. Liao SJ. On the homotopy analysis method for nonlinear problems. *Applied Mathematics and Computation* 2004; **147**(2):499–513.
21. Liao SJ. A non-iterative numerical approach for two-dimensional viscous flow problems governed by the Falkner–Skan equation. *International Journal for Numerical Methods in Fluids* 2001; **35**(5):495–518.
22. Liao SJ, Campo A. Analytic solutions of the temperature distribution in Blasius viscous flow problems. *Journal of Fluid Mechanics* 2002; **453**:411–425.
23. Liao SJ. On the analytic solution of magnetohydrodynamics flows of non-Newtonian fluids over a stretching sheet. *Journal of Fluid Mechanics* 2003; **488**:189–212.
24. Liao SJ, Cheung KF. Homotopy analysis of nonlinear progressive waves in deep water. *Journal of Engineering Mathematics* 2003; **45**(2):105–116.

DOI: 10.1002/fld

25. Abbasbandy S. The application of homotopy analysis method to solve a generalized Hirota–Satsuma coupled KdV equation. *Physics Letters A* 2007; **361**:478–483.
26. Hayat T, Sajid M. On analytic solution for thin film flow of a fourth grade fluid down a vertical cylinder. *Physics Letters A* 2007; **361**:316–322.
27. Zhu SP. An exact and explicit solution for the valuation of American put options. *Quantitative Finance* 2006; **6**(3):229–242.
28. Liao SJ, Chwang AT. General boundary element method for nonlinear problems. *International Journal for Numerical Methods in Fluids* 1996; **23**(5):467–483.
29. Wu YY, Liao SJ. Solving high Reynolds-number viscous flows by the general BEM and domain decomposition method. *International Journal for Numerical Methods in Fluids* 2005; **47**(3):185–199.
30. Toro EF. *Shock-capturing Methods for Free-surface Shallow Flows*. Wiley: Chichester, U.K., 2001.
31. Johnson WP. The curious history of Faà di Bruno's formula. *American Mathematical Monthly* 2002; **109**(3): 217–234.
32. Liang Q, Borthwick AGL, Stelling G. Simulation of dam- and dyke-break hydrodynamics on dynamically adaptive quadtree grids. *International Journal for Numerical Methods in Fluids* 2004; **46**(2):127–162.
33. Alcrudo F, Garcia-Navarro P. A high-resolution Godunov-type scheme in finite volumes for the 2D shallow-water equations. *International Journal for Numerical Methods in Fluids* 1993; **16**(6):489–505.
34. Billett SJ, Toro EF. On WAF-type schemes for multidimensional hyperbolic conservation laws. *Journal of Computational Physics* 1997; **130**(1):1–24.
35. Mingham CG, Causon DM. High-resolution finite-volume method for shallow water flows. *Journal of Hydraulic Engineering* 1998; **124**(6):605–614.
36. Toro EF, Titarev VA. Solution of the generalized Riemann problem for advection–reaction equations. *Proceedings of the Royal Society of London, Series A* 2002; **458**(2018):271–281.
37. Castro CE, Toro EF. A Riemann solver and upwind methods for a two-phase flow model in non-conservative form. *International Journal for Numerical Methods in Fluids* 2006; **50**(3):275–307.
38. Giacomazzo B, Rezzolla L. The exact solution of the Riemann problem in relativistic magnetohydrodynamics. *Journal of Fluid Mechanics* 2006; **562**:223–259.

DOI: 10.1002/fld